ACS Photonics

pubs.acs.org/journal/apchd5

Article

Decoupled Phase Modulation for Circularly Polarized Light via Chiral Metasurfaces

Renchao Jin, Lin Deng, Lili Tang, Yue Cao, Yongmin Liu,* and Zheng-Gao Dong*

Cite This: *ACS Photonics* 2023, 10, 155−161

Read Online

ACCESS | Metrics & More | Article Recommendations | Supporting Information

ABSTRACT: Metasurfaces have emerged as one highly vibrant frontier in the field of nanophotonics, since they enable some unique and practical means to modulate the phase, polarization, angular momentum, and spatial field distribution through structural engineering. However, the current methods of phase modulation based on the propagation phase and Pancharatnam−Berry phase are typically interrelated between two eigen spin states for each single-step modulation. It means that when the phase of left-handed circularly polarized (LCP) light is modulated by a metasurface, the phase of right-handed circularly polarized (RCP) light will change as well, imposing substantial constraints if spin-decoupled or spin-independent applications are sought. In this paper, we numerically and experimentally demonstrate a new phase modulation pathway based on chiral metasurfaces consisting of V-shaped plasmonic apertures, which enable fully decoupled phase modulation for the two eigen spin states. Two enantiomers are proposed to achieve the desired phase decoupling. Specifically, the enantiomer can manipulate the phase of the LCP component of a light beam without changing the phase of the RCP component, and vice versa. Our method expands the methods of phase engineering and can help us design novel devices for a wide range of applications, including polarimetric imaging, chiroptical detection, molecular spectroscopy, and quantum information processing.

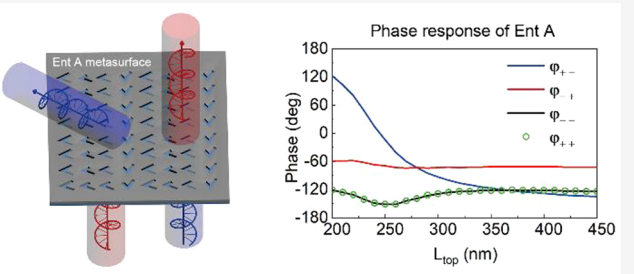

KEYWORDS: *metasurfaces, photonic spin Hall effect, plasmonics, chirality, nanophotonics, circular dichroism*

INTRODUCTION

On-demand manipulation of electromagnetic waves is crucial for the development of modern technologies. Metasurfaces, planar metamaterials with a subwavelength thickness that allow us to flexibly manipulate electromagnetic waves, have been widely studied over the past decade.[1−3] Metasurfaces can modulate the amplitude, phase, polarization, and angular momentum of electromagnetic waves. Among these properties, phase modulation is of much interest, which has led to beam steering,[4−6] holograms,[7−11] flat lenses,[12−14] and so on. It is relatively straightforward to achieve selective control of the phase of a linearly polarized beam by changing the geometric parameters of the subwavelength meta-atoms.[1] Thereafter, a single metasurface with multiple and independent phase modulations for different linearly polarized light (i.e., transverse magnetic and transverse electric modes) was investigated for a variety of applications.[15−17] Recently, the phase modulation of LCP and RCP light has attracted much attention, since these two orthogonal eigen spin states can produce many interesting phenomena and applications while interacting with matter, such as chiral sensing and sorting,[18−21] polarization imaging,[22,23] information coding,[24−27] and spin-to-orbital angular momentum conversion.[28−30]

The conventional methods to manipulate the phase of LCP and RCP light are generally based on the propagation phase and Pancharatnam−Berry (PB) phase modulation.[31−40] The former is related to the geometric parameters of subwavelength meta-atoms and always imparts the same phase modulation to LCP and RCP light simultaneously.[31] Due to its identical phase modulation for LCP and RCP incidences, the propagation phase is a good candidate for circular-polarization insensitive devices.[41,42] In contrast, the PB phase imparts different phase modulation for LCP and RCP light, with the same magnitude but opposite signs. Therefore, the PB phase modulation is used to split LCP and RCP light. For example, people have studied the photonic spin Hall effect using the metasurface platform.[34,43,44] However, both the propagation phase and the PB phase modulation approaches have their own limitations, and we can hardly decouple the phase modulation for LCP and RCP lights by either approach (i.e., modulating LCP phase while leaving RCP phase unchanged by propagation phase or PB phase, or vice versa), though the independent control for linearly and orthogonally polarized

Received: September 6, 2022
Published: December 27, 2022

https://doi.org/10.1021/acsphotonics.2c01397
ACS Photonics 2023, 10, 155−161

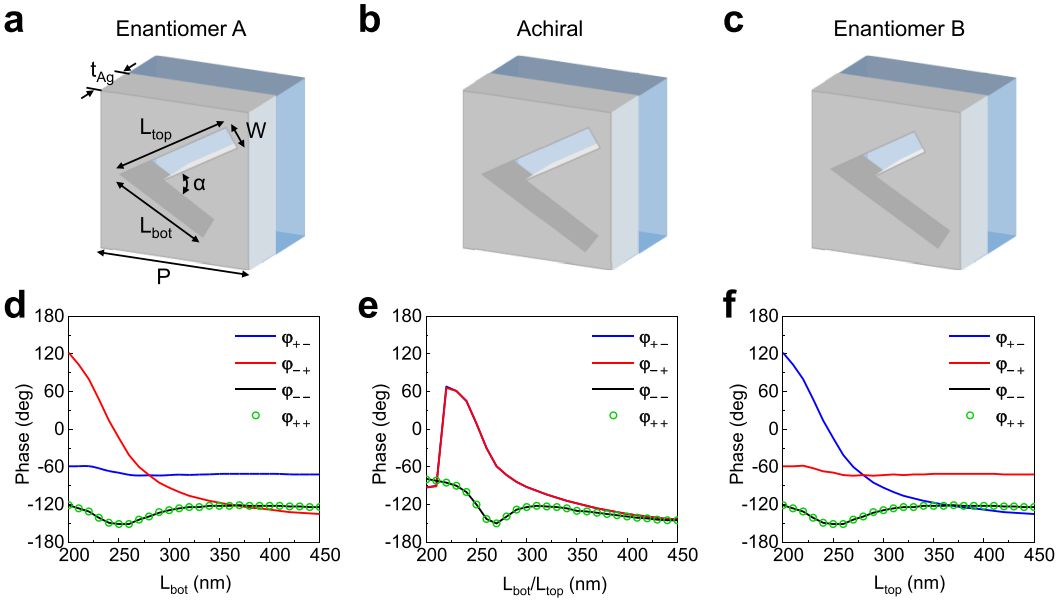

Figure 1. (a–c) Schematics of (a) enantiomer A, (b) achiral, and (c) enantiomer B apertures. (d–f) The corresponding phase responses of the apertures in (a–c) at a wavelength of 1064 nm. In (d) the length of top arm L_{top} is fixed at 430 nm, while in (f) the length of bottom arm L_{bot} is fixed at 430 nm.

light can be easily achieved by using anisotropic structures.[15−17] Fortunately, by combining propagation and PB phases, the arbitrary phase modulation for LCP and RCP light has been achieved, which has expanded the fields of spin-dependent optical devices.[31−35] Even though this combination method can manipulate the phase of LCP and RCP light simultaneously, there is still a pressing need to find an alternative way to completely decouple the phase modulation for these two spin states of light.

DESIGN AND SIMULATIONS

In this paper, we demonstrate a new approach to decouple the phase of LCP and RCP light using chiral metasurfaces, which can uniquely manipulate the phase of either LCP or RCP light. For example, we can achieve independent modulation of the LCP phase by single-step modulation while keeping the RCP phase unchanged, which is not possible in conventional methods.[31−40]

The concept of decoupled phase of LCP and RCP light can be understood by considering the Jones matrix of nanostructures under circularly polarized base of light as follows:[23]

$$J = R(\theta)^{-1}\begin{vmatrix} A_{RR}e^{i\varphi_{RR}} & A_{RL}e^{i\varphi_{RL}} \\ A_{LR}e^{i\varphi_{LR}} & A_{LL}e^{i\varphi_{LL}} \end{vmatrix} R(\theta) \quad (1)$$

where $R(\theta)$ is the rotation matrix corresponding to the in-plane rotation of the nanostructures (i.e., directly related to the PB phase), A and φ are the amplitude and phase, respectively, and the subscript of R/L refers to the RCP/LCP. In general, the Jones matrix in eq 1 should have four independent components. However, in most cases, the phase of crossed polarized light are always the same (i.e., $\varphi_{RL} = \varphi_{LR}$), which can be regarded as the coupled phase, inevitably limiting the functionalities of LCP and RCP light. Therefore, an arbitrarily customized Jones matrix is needed to break the coupled phase.

In this work, we propose a novel way to decouple the phase of crossed polarization of LCP and RCP light, by using chiral V-shaped apertures to realize the decoupled phase of $\varphi_{RL} \neq \varphi_{LR}$. In addition, φ_{RL} and φ_{LR} can be arbitrarily customized, after breaking their coupling.

As shown in Figure 1a, the V-shaped aperture is etched in a silver film with thickness t_{Ag} = 40 nm by focused ion beam system (FEI, FIB 200). The opening angle of the aperture is α = 60°, the periodicity of the metasurface is P = 450 nm, and the substrate is silica. The V-shaped aperture has two tunable arms, i.e., the top arm L_{top} and bottom arm L_{bot}, and an identical width W = 100 nm. Figure 1a-c illustrate the schematics of two enantiomers and an achiral aperture. Specifically, the V-shaped aperture with tunable bottom arm L_{bot} is enantiomer A (Ent A), while its length of top arm L_{top} is fixed at 430 nm, as shown in Figure 1a. In Figure 1b, the achiral V-shaped aperture has two tunable arms of the same length. Enantiomer B (Ent B) in Figure 1c has an adjustable top arm L_{top} while the length of bottom arm L_{bot} is fixed at 430 nm, showing the opposite chirality in comparison with enantiomer A. Depending on the geometry, these apertures have different phase responses. We have investigated their phase responses under LCP and RCP illumination at a wavelength of 1064 nm by commercial electromagnetic solver CST Studio Suite. The simulation results are shown in Figures 1d–f. Throughout the remaining of the paper, we denote LCP and RCP light as − and + , respectively. For example, symbol φ_{+-} represents the phase of the transmitted RCP component under the incidence of LCP light. We can find that Ent A has a large phase variation in response to the change of L_{bot} when the incidence is RCP light (red line in Figure 1d). As for its counterpart, the rapidly changed blue line in Figure 1f indicates that Ent B is sensitive to LCP incidence. The results in Figure 1e for an achiral V-shape aperture show identical phase responses to LCP and RCP light. Therefore, the simulation results presented here demonstrate the feasibility to decouple the phase modulations of LCP and RCP light using Ent A and Ent B, elucidating a clear distinction from the achiral aperture. We want to emphasize that the enantiomers have no obvious circular dichroism,[37,45−49] since the amplitudes of transmission for LCP and RCP incidences almost keep the

https://doi.org/10.1021/acsphotonics.2c01397
ACS Photonics 2023, 10, 155−161

same (see Figure S1 in the Supporting Information). Instead, the phase response of the enantiomer pair shows a phenomenon similar to "circular dichroism". The same transmission amplitude but different phase response is desirable for chiroptical sensors using chiral metasurfaces, as it can suppress the background circular dichroism signals from the metasurfaces.[50,51]

To reveal the underlying mechanism of spin-decoupled phase modulation in Figure 1, we have simulated the magnetic field distributions of three types of V-shaped apertures, as shown in Figure 2. For the achiral aperture, the magnetic field shows

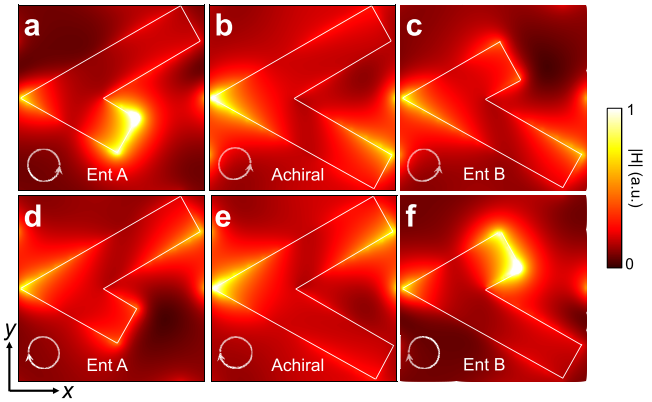

Figure 2. (a–c) Magnetic field distribution in Ent A (a), achiral aperture (b), and Ent B (c) for RCP incidence. (d–f) Magnetic field distribution in Ent A (d), achiral aperture (e), and Ent B (f) for LCP incidence. The fields are plotted in the plane 10 nm above the surface. The long arm is 430 nm, while the short arm is 260 nm. Counterclockwise circles indicate RCP incidence and clockwise circles indicate LCP incidence.

obviously different distributions depending on the handedness of incidence. Intriguingly, the magnetic field of achiral aperture is more concentrated in the bottom/top arm with RCP/LCP incidence (Figure 2b,e). Therefore, when we decrease the length of the bottom arm (i.e., Ent A), the magnetic field distribution changes significantly for RCP incidence, resulting in a larger local field enhancement in the bottom arm (Figure 2a). However, when irradiated with LCP light, the magnetic field distribution (Figure 2d) in the top arm of Ent A is very similar to that of the achiral structure (Figure 2e), even though the length of the bottom arm is reduced. As a result, changing the bottom arm has negligible effect on the phase of LCP incidence. On the contrary, Ent B shows a concentrated magnetic field in the top arm while illuminated with LCP light (Figure 2f), and hence, the top arm can independently control the phase of LCP incidence. To conclude, these chiral near field distribution of Ent A and Ent B are strictly dependent on the chirality of incident light, leading to the independent control of the phase response of RCP and LCP incidence. The spin-decoupled phase modulation on the basis of our enantiomers is different from the PB-phase modulation or propagation-phase modulation, which imposes opposite or identical phase rather than arbitrary phases. It is noted that the chiral near field distribution presented in the achiral V-shaped antennas has been well studied.[49,50] The reason is attributed to the interference of resonant modes in the V-shaped antenna.

To explicitly demonstrate the spin-decoupled phase modulation of the enantiomers, we have simulated the phase diagrams φ and transmitted amplitudes of RCP and LCP incidences at 1064 nm for the cross-polarized components. The results are depicted in Figure 3. It is apparent that the

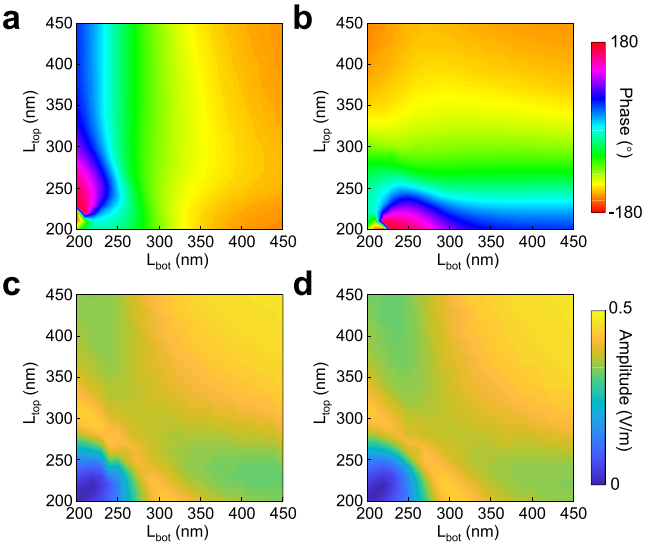

Figure 3. Phase diagrams for the cross-polarized component of transmitted light, when the metasurface is subject to (a) RCP incidence, and (b) LCP incidence. Amplitude for the cross-polarized component of transmitted light, when the metasurface is subject to (c) RCP incidence and (d) LCP incidence.

amplitude distributions (Figure 3c,d) of LCP and RCP incidences almost keep the same. However, the phase responses (Figure 3a,b) of LCP and RCP incidences show significant differences, as they vary along the vertical and horizontal directions, respectively. In most areas of Figure 3a, the phase modulation of RCP incidence shows continuous phase gradients along the horizontal direction but almost the same values along the vertical direction, indicating that L_{bot} plays an important role in the phase modulation for RCP incidence. While for LCP incidence presented in Figure 3b, the trend is opposite to Figure 3a, that is, L_{top} can modulate the phase of LCP incidence. These results suggest that we can achieve fully decoupled phase modulation for the RCP/LCP incidences by designing some specific enantiomers. Our enantiomer design strategy is simpler than the existing methods, which rely on the combination of propagation phase and PB phase to achieve spin-decoupled phase modulation.[31−40] The spin-decoupled phase modulation of enantiomers provides another degree of freedom in phase engineering, which can open new ways to design metasurface and ease the design and fabrication.

EXPERIMENTAL DEMONSTRATION

In the following, we apply the spin-decoupled phase modulation to design functional devices. As a proof-of-principle demonstration, three metasurfaces using arrays of Ent A, Ent B, and achiral apertures have been designed and fabricated to validate our theoretical analysis. The scanning electron microscope (SEM) images of the samples are shown in Figure 4a, d, and g, respectively. Each metasurfaces consists of four apertures to form a phase gradient of $d\varphi/dx = \pi/2P$ along + x direction for the corresponding incidence. For example, the Ent A metasurface has four Ent A apertures (red box in Figure 4a), with L_{bot} equals 430, 260, 200, and 260 nm, respectively. Therefore, Ent A metasurface represents the

https://doi.org/10.1021/acsphotonics.2c01397
ACS Photonics 2023, 10, 155−161

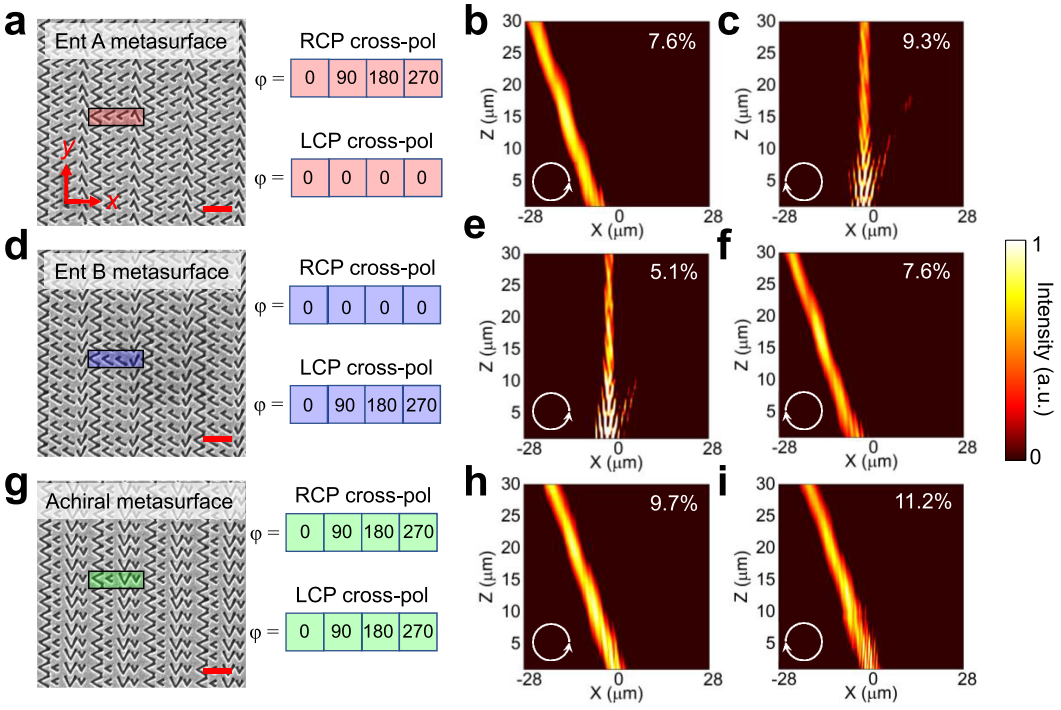

Figure 4. SEM image of the fabricated (a) Ent A metasurface, (d) Ent B metasurface, and (g) achiral metasurface. The red, blue, and green boxes indicate the supercell of the individual metasurface. The phase gradients of RCP cross-pol and LCP cross-pol are plotted on the right side. Scale bar: 1 μm. Measured cross-polarized transmission with RCP incidence for (b) Ent A metasurface, (e) Ent B metasurface, and (h) achiral metasurface, respectively. Measured cross-polarized transmission with LCP incidence for (c) Ent A metasurface, (f) Ent B metasurface, and (i) achiral metasurface, respectively. The measured efficiencies of the metasurfaces are shown at the upper right corners.

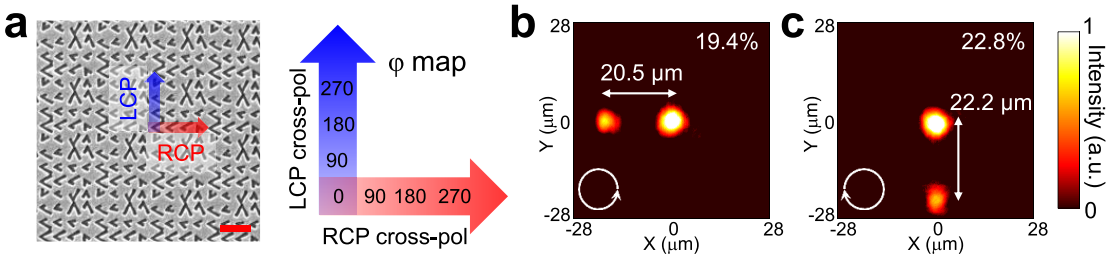

Figure 5. (a) SEM image of the chiral metasurface to achieve dual refractions for RCP and LCP light. (b, c) Measured intensity distribution at plane 30 μm above the metasurfaces for RCP and LCP incidences, respectively. The measured efficiencies of the metasurfaces are shown at the upper right corners.

phase of RCP cross-pol (cross-polarized light when the incidence is RCP) φ = 0°, 90°, 180°, and 270°, and always φ = 0 of LCP cross-pol (cross-polarized light when the incidence is LCP). With this specific arrangement, the Ent A metasurface deflects only the LCP component (i.e., cross-polarization) of the transmitted light when the incidence is RCP. The fourth aperture in Ent A has a rotation angle of 90°, to achieve a phase increment of 270° relative to the first aperture in Ent A. The additional rotation angle is a trade-off due to the limited modulation range of the decoupled phase for single-layered metallic structures, while this limitation can be eased by multilayered structures. However, it is worth noting that the decoupled phase itself still works well with an additional 90° rotation, whereas the previous methods required flexible rotation angles. Then, we experimentally characterized the metasurface using a homemade setup (see Figure S2 in the Supporting Information). The measured cross-polarized components of transmitted light of Ent A metasurface are shown in Figure 4b,c. It is clear that for RCP incidence, the detected LCP component of transmitted light has an obvious deflection. The refraction angle in Figure 4b is 35.8°, in excellent agreement with our expectation (36.2°). However, if we flip the polarization of the input laser beam to LCP, the RCP component of the transmitted light shows a refraction angle of 0°, as presented in Figure 4c. As a counterpart of Ent A metasurface, the measured results of Ent B metasurface (Figure 4d) are exactly opposite. The RCP incidence has a refraction angle of 0° (Figure 4e), and the deflection of the LCP incidence in Figure 4f is the same as that in Figure 4b. As a comparison, the cross-polarized component of the transmitted light through the achiral metasurface (Figure 4g) has the same deflection angle regardless of RCP and LCP incidences, as shown in Figure 4h,i. The results of copolarized transmission are presented in Figure S3 of the Supporting Information, demonstrating that all three metasurfaces have no deflection for copolarized components. In addition, the measured efficiency in Figure 4b is about 7.6% (calculated by the transmitted power of polarized channel compared to the

https://doi.org/10.1021/acsphotonics.2c01397
ACS Photonics 2023, 10, 155−161

input power), while the efficiency in Figure 4c is about 9.3%. Compared to the 15% efficiency in our simulations, the slightly lower efficiency in measurements is mainly due to the imperfection of samples. The efficiency can be further enhanced by using a dielectric metasurface or a reflective metasurface, in which the spin-decoupled phase modulation is still applicable. Moreover, the metasurfaces have considerable bandwidth of around 200 nm, as shown in Figure S4 of the Supporting Information.

With the ability to control the phase of LCP and RCP light independently, the proposed spin-decoupled phase modulation has its novelty in comparison to the conventional method that combines the propagation phase and the PB phase. For example, as shown in Figure 5a, we have designed a chiral metasurface that can simultaneously deflect light into horizontal/vertical directions for RCP/LCP incidences. It is noted that some enantiomers have in-plane rotation in order to further boost the functionality of our devices. The red and blue arrows denote the phase gradient directions for RCP and LCP light, respectively. On the right side of Figure 5a, the phase distributions of RCP cross-pol and LCP cross-pol are plotted along horizontal and vertical directions, respectively. The phase interval between two neighboring apertures equals 90°, corresponding to a designed refraction angle of 36.2°. In order to detect the refraction along the horizontal and vertical directions simultaneously, we collected transmitted light without a polarization filter. In other words, we collected transmitted light with co- and cross-polarizations. The results obtained with the polarization filter can be found in Figure S5 of the Supporting Information. As shown in Figure 5b and c, we extracted the intensity at $z = 30$ μm plane, the efficiencies of the metasurface is 19.4% and 22.8% for RCP and LCP incidence, respectively. The central bright spot in Figure 5b,c represents directly transmitted light with a refraction angle of 0°, while the relatively weak spot is the deflected light with cross-polarization. The 20.5 μm displacement of the two spots along the horizontal direction in Figure 5b implies a refraction angle of 34.3°, which is slightly smaller than the refraction angle of our theoretical prediction (36.2°). In addition, the 22.2 μm displacement along the vertical direction in Figure 5c represents an angle of 36.3°, which is in good agreement with our theoretically expected refraction angle. Overall, the chiral metasurface shows two-dimensional beam steering for both RCP and LCP incidences, confirming that our enantiomers can achieve independent functions subject to RCP and LCP incidences.

CONCLUSION

In conclusion, we have proposed a new method to decouple the phase responses of RCP and LCP light. The key feature of this spin-decoupled phase modulation originates from V-shaped apertures that support chiral near-field distributions. To demonstrate the proposed spin-decoupled phase modulation, we first designed and fabricated the Ent A and Ent B metasurfaces, allowing anomalous refraction only for the transmitted cross-polarized component of RCP or LCP incidence. Then we demonstrated a chiral metasurface showing anomalous refraction along the horizontal/vertical directions for RCP/LCP light. The measured results of our fabricated chiral metasurfaces and theoretical results match each other very well, validating the capability of spin-decoupled phase modulation by our proposed enantiomers. The results presented here have significant implications in the field of metasurfaces to expand the horizon of phase engineering, which would enable novel spin-based meta-devices, including polarization imaging, optical manipulation, holograms, and sensing.

ASSOCIATED CONTENT

Supporting Information

The Supporting Information is available free of charge at https://pubs.acs.org/doi/10.1021/acsphotonics.2c01397.

Further details on the transmission of enantiomers, the homemade optical setup, measured copolarization results, simulated bandwidth, and polarized images (PDF)

AUTHOR INFORMATION

Corresponding Authors

Yongmin Liu − *Department of Electrical and Computer Engineering, Northeastern University, Boston, Massachusetts 02115, United States; Department of Mechanical and Industrial Engineering, Northeastern University, Boston, Massachusetts 02115, United States;* orcid.org/0000-0003-1084-6651; Email: y.liu@northeastern.edu

Zheng-Gao Dong − *School of Physics, Southeast University, Nanjing 211189, China;* orcid.org/0000-0003-1655-0253; Email: zgdong@seu.edu.cn

Authors

Renchao Jin − *School of Physics, Southeast University, Nanjing 211189, China;* orcid.org/0000-0001-9256-322X

Lin Deng − *Department of Electrical and Computer Engineering, Northeastern University, Boston, Massachusetts 02115, United States*

Lili Tang − *School of Physics, Southeast University, Nanjing 211189, China*

Yue Cao − *School of Physics, Southeast University, Nanjing 211189, China*

Complete contact information is available at: https://pubs.acs.org/10.1021/acsphotonics.2c01397

Funding

Z.G. acknowledges the financial support of National Natural Science Foundation of China (12174052). Y.L. acknowledges the financial support of the National Science Foundation (ECCS-1916839, CBET-1931777, and ECCS-2136168)

Notes

The authors declare no competing financial interest.

REFERENCES

(1) Yu, N.; Genevet, P.; Kats, M. A.; Aieta, F.; Tetienne, J. P.; Capasso, F.; Gaburro, Z. Light Propagation with Phase Discontinuities: Generalized Laws of Reflection and Refraction. *Science* **2011**, *334*, 333−337.

(2) Yu, N.; Capasso, F. Flat Optics with Designer Metasurfaces. *Nat. Mater.* **2014**, *13*, 139−150.

(3) Kildishev, A. V.; Boltasseva, A.; Shalaev, V. M. Planar Photonics with Metasurfaces. *Science* **2013**, *339*, 1232009.

(4) Ni, X.; Emani, N. K.; Kildishev, A. V.; Boltasseva, A.; Shalaev, V. M. Broadband Light Bending with Plasmonic Nanoantennas. *Science* **2012**, *335*, 427−427.

(5) Sun, S.; Yang, K. Y.; Wang, C. M.; Juan, T. K.; Chen, W. T.; Liao, C. Y.; He, Q.; Xiao, S.; Kung, W. T.; Guo, G. Y.; Zhou, L.; Tsai,

D. P. High-Efficiency Broadband Anomalous Reflection by Gradient Meta-Surfaces. *Nano Lett.* **2012**, *12*, 6223−6229.
(6) Ding, F.; Deshpande, R.; Bozhevolnyi, S. I. Bifunctional Gap-Plasmon Metasurfaces for Visible Light: Polarization-Controlled Unidirectional Surface Plasmon Excitation and Beam Steering at Normal Incidence. *Light: Sci. Appl.* **2018**, *7*, 17178.
(7) Zheng, G.; Mühlenbernd, H.; Kenney, M.; Li, G.; Zentgraf, T.; Zhang, S. Metasurface Holograms Reaching 80% Efficiency. *Nat. Nanotechnol.* **2015**, *10*, 308−312.
(8) Huang, L.; Zhang, S.; Zentgraf, T. Metasurface Holography: From Fundamentals to Applications. *Nanophotonics* **2018**, *7*, 1169−1190.
(9) Genevet, P.; Capasso, F. Holographic Optical Metasurfaces: A review of Current Progress. *Rep. Prog. Phys.* **2015**, *78*, 024401.
(10) Ma, W.; Xu, Y.; Xiong, B.; Deng, L.; Peng, R. W.; Wang, M.; Liu, Y. Pushing the Limits of Functionality-Multiplexing Capability in Metasurface Design Based on Statistical Machine Learning. *Adv. Mater.* **2022**, *34*, 2110022.
(11) Xiong, B.; Xu, Y.; Wang, J.; Li, L.; Deng, L.; Cheng, F.; Peng, R. W.; Wang, M.; Liu, Y. Realizing Colorful Holographic Mimicry by Metasurfaces. *Adv. Mater.* **2021**, *33*, 2005864.
(12) Khorasaninejad, M.; Chen, W. T.; Devlin, R. C.; Oh, J.; Zhu, A. Y.; Capasso, F. Metalenses at Visible Wavelengths: Diffraction-Limited Focusing and Subwavelength Resolution Imaging. *Science* **2016**, *352*, 1190−1194.
(13) Chen, X.; Huang, L.; Mühlenbernd, H.; Li, G.; Bai, B.; Tan, Q.; Jin, G.; Qiu, C. W.; Zhang, S.; Zentgraf, T. Dual-Polarity Plasmonic Metalens for Visible Light. *Nat. Commun.* **2012**, *3*, 1−6.
(14) Khorasaninejad, M.; Capasso, F. Metalenses: Versatile Multifunctional Photonic Components. *Science* **2017**, *358*, No. eaam8100.
(15) Arbabi, A.; Horie, Y.; Bagheri, M.; Faraon, A. Dielectric Metasurfaces for Complete Control of Phase and Polarization with Subwavelength Spatial Resolution and High Transmission. *Nat. Nanotechnol.* **2015**, *10*, 937−943.
(16) Xu, Y.; Li, Q.; Zhang, X.; Wei, M.; Xu, Q.; Wang, Q.; Zhang, H.; Zhang, W.; Hu, C.; Zhang, Z.; Zhang, C.; Zhang, X.; Han, J.; Zhang, W. Spin-decoupled multifunctional metasurface for asymmetric polarization generation. *ACS Photonics* **2019**, *6*, 2933−2941.
(17) Wu, T.; Zhang, X.; Xu, Q.; Plum, E.; Chen, K.; Xu, Y.; Lu, Y.; Zhang, H.; Zhang, Z.; Chen, X.; Ren, G.; Niu, L.; Tian, Z.; Han, J.; Zhang, W. Dielectric metasurfaces for complete control of phase, amplitude, and polarization. *Adv. Opt. Mater.* **2022**, *10*, 2101223.
(18) Solomon, M. L.; Hu, J.; Lawrence, M.; García-Etxarri, A.; Dionne, J. A. Enantiospecific Optical Enhancement of Chiral Sensing and Separation with Dielectric Metasurfaces. *ACS Photonics* **2019**, *6*, 43−49.
(19) Yao, K.; Liu, Y. Enhancing Circular Dichroism by Chiral Hotspots in Silicon Nanocube Dimers. *Nanoscale* **2018**, *10*, 8779−8786.
(20) Huang, Z.; Yao, K.; Su, G.; Ma, W.; Li, L.; Liu, Y.; Zhan, P.; Wang, Z. Graphene-metal hybrid metamaterials for strong and tunable circular dichroism generation. *Opt. Lett.* **2018**, *43*, 2636.
(21) Zhang, T.; Mahdy, M. R. C.; Liu, Y.; Teng, J. H.; Lim, C. T.; Wang, Z.; Qiu, C.-W. All-Optical Chirality-Sensitive Sorting via Reversible Lateral Forces in Interference Fields. *ACS Nano* **2017**, *11*, 4292−4300.
(22) Khorasaninejad, M.; Chen, W. T.; Zhu, A. Y.; Oh, J.; Devlin, R. C.; Rousso, D.; Capasso, F. Multispectral Chiral Imaging with a Metalens. *Nano Lett.* **2016**, *16*, 4595−4600.
(23) Rubin, N. A.; D'Aversa, G.; Chevalier, P.; Shi, Z.; Chen, W. T.; Capasso, F. Matrix Fourier Optics Enables a Compact Full-Stokes Polarization Camera. *Science* **2019**, *365*, No. eaax1839.
(24) Chen, P.; Ge, S. J.; Duan, W.; Wei, B. Y.; Cui, G. X.; Hu, W.; Lu, Y. Q. Digitalized Geometric Phases for Parallel Optical Spin and Orbital Angular Momentum Encoding. *ACS Photonics* **2017**, *4*, 1333−1338.
(25) Dong, F.; Feng, H.; Xu, L.; Wang, B.; Song, Z.; Zhang, X.; Yan, L.; Li, X.; Tian, Y.; Wang, W.; Sun, L.; Li, Y.; Chu, W. Information Encoding with Optical Dielectric Metasurface via Independent Multichannels. *ACS Photonics* **2019**, *6*, 230−237.
(26) Jin, L.; Dong, Z.; Mei, S.; Yu, Y. F.; Wei, Z.; Pan, Z.; Rezaei, S. D.; Li, X.; Kuznetsov, A. I.; Kivshar, Y. S.; Yang, J. K. W.; Qiu, C. W. Noninterleaved Metasurface for (2^6 −1) Spin- and Wavelength-Encoded Holograms. *Nano Lett.* **2018**, *18*, 8016−8024.
(27) Shu, F. Z.; Wang, J. N.; Peng, R. W.; Xiong, B.; Fan, R. H.; Gao, Y. J.; Liu, Y.; Qi, D. X.; Wang, M. Electrically Driven Tunable Broadband Polarization States Via Active Metasurfaces Based on Joule-Heat-Induced Phase Transition of Vanadium Dioxide. *Laser Photonics Rev.* **2021**, *15* (10), 2100155.
(28) Xiao, S.; Wang, J.; Liu, F.; Zhang, S.; Yin, X.; Li, J. Spin-Dependent Optics with Metasurfaces. *Nanophotonics* **2017**, *6*, 215−234.
(29) Devlin, R. C.; Ambrosio, A.; Wintz, D.; Oscurato, S. L.; Zhu, A. Y.; Khorasaninejad, M.; Oh, J.; Maddalena, P.; Capasso, F. Spin-to-Orbital Angular Momentum Conversion in Dielectric Metasurfaces. *Opt. Express* **2017**, *25*, 377.
(30) Bliokh, K. Y.; Rodríguez-Fortuño, F. J.; Nori, F.; Zayats, A. v. Spin-Orbit Interactions of Light. *Nat. Photonics* **2015**, *9*, 796−808.
(31) Balthasar Mueller, J. P.; Rubin, N. A.; Devlin, R. C.; Groever, B.; Capasso, F. Metasurface Polarization Optics: Independent Phase Control of Arbitrary Orthogonal States of Polarization. *Phys. Rev. Lett.* **2017**, *118*, 113901.
(32) Devlin, R. C.; Ambrosio, A.; Rubin, N. A.; Mueller, J. P. B.; Capasso, F. Arbitrary Spin-to-Orbital Angular Momentum Conversion of Light. *Science* **2017**, *358*, 896−901.
(33) Li, S.; Li, X.; Wang, G.; Liu, S.; Zhang, L.; Zeng, C.; Wang, L.; Sun, Q.; Zhao, W.; Zhang, W. Multidimensional Manipulation of Photonic Spin Hall Effect with a Single-Layer Dielectric Metasurface. *Adv. Opt. Mater.* **2019**, *7*, 1801365.
(34) Jin, R.; Tang, L.; Li, J.; Wang, J.; Wang, Q.; Liu, Y.; Dong, Z. G. Experimental Demonstration of Multidimensional and Multifunctional Metalenses Based on Photonic Spin Hall Effect. *ACS Photonics* **2020**, *7*, 512−518.
(35) Xu, H. X.; Han, L.; Li, Y.; Sun, Y.; Zhao, J.; Zhang, S.; Qiu, C. W. Completely Spin-Decoupled Dual-Phase Hybrid Metasurfaces for Arbitrary Wavefront Control. *ACS Photonics* **2019**, *6*, 211−220.
(36) Bai, G. D.; Ma, Q.; Li, R. Q.; Mu, J.; Jing, H. B.; Zhang, L.; Cui, T. J. Spin-Symmetry Breaking Through Metasurface Geometric Phases. *Phys. Rev. Appl.* **2019**, *12*, 044042.
(37) Xu, H. X.; Hu, G.; Li, Y.; Han, L.; Zhao, J.; Sun, Y.; Yuan, F.; Wang, G. M.; Jiang, Z. H.; Ling, X.; Cui, T. J.; Qiu, C. W. Interference-Assisted Kaleidoscopic Meta-Plexer for Arbitrary Spin-Wavefront Manipulation. *Light: Sci. Appl.* **2019**, *8*, 3.
(38) Chen, X.; Chen, M.; Mehmood, M. Q.; Wen, D.; Yue, F.; Qiu, C. W.; Zhang, S. Longitudinal Multifoci Metalens for Circularly Polarized Light. *Adv. Opt. Mater.* **2015**, *3*, 1201−1206.
(39) Chen, C.; Gao, S.; Song, W.; Li, H.; Zhu, S.-N.; Li, T. Metasurfaces with Planar Chiral Meta-Atoms for Spin Light Manipulation. *Nano Lett.* **2021**, *21*, 1815−1821.
(40) Wang, Q.; Plum, E.; Yang, Q.; Zhang, X.; Xu, Q.; Xu, Y.; Han, J.; Zhang, W. Reflective chiral meta-holography: multiplexing holograms for circularly polarized waves. *Light: Sci. Appl.* **2018**, *7* (1), 25.
(41) Arbabi, A.; Horie, Y.; Ball, A. J.; Bagheri, M.; Faraon, A. Subwavelength-Thick Lenses with High Numerical Apertures and Large Efficiency Based on High-Contrast Transmitarrays. *Nat. Commun.* **2015**, *6*, 7069.
(42) Wang, W.; Guo, Z.; Li, R.; Zhang, J.; Li, Y.; Liu, Y.; Wang, X.; Qu, S. Plasmonics Metalens Independent from the Incident Polarizations. *Opt. Express* **2015**, *23*, 16782.
(43) Zhou, J.; Qian, H.; Hu, G.; Luo, H.; Wen, S.; Liu, Z. Broadband Photonic Spin Hall Meta-Lens. *ACS Nano* **2018**, *12*, 82−88.
(44) Ling, X.; Zhou, X.; Huang, K.; Liu, Y.; Qiu, C. W.; Luo, H.; Wen, S. Recent Advances in the Spin Hall Effect of Light. *Rep. Prog. Phys.* **2017**, *80*, 066401.

https://doi.org/10.1021/acsphotonics.2c01397
ACS Photonics 2023, 10, 155−161

(45) Ma, Z.; Li, Y.; Li, Y.; Gong, Y.; Maier, S. A.; Hong, M. All-Dielectric Planar Chiral Metasurface with Gradient Geometric Phase. *Opt. Express* **2018**, *26*, 6067.
(46) Jing, L.; Wang, Z.; Maturi, R.; Zheng, B.; Wang, H.; Yang, Y.; Shen, L.; Hao, R.; Yin, W.; Li, E.; Chen, H. Gradient Chiral Metamirrors for Spin-Selective Anomalous Reflection. *Laser Photonics Rev.* **2017**, *11*, 1700115.
(47) Wang, Z.; Jing, L.; Yao, K.; Yang, Y.; Zheng, B.; Soukoulis, C. M.; Chen, H.; Liu, Y. Origami-Based Reconfigurable Metamaterials for Tunable Chirality. *Adv. Mater.* **2017**, *29*, 1700412.
(48) Kang, L.; Rodrigues, S. P.; Taghinejad, M.; Lan, S.; Lee, K.-T.; Liu, Y.; Werner, D. H.; Urbas, A.; Cai, W. Preserving Spin States upon Reflection: Linear and Nonlinear Responses of a Chiral Meta-Mirror. *Nano Lett.* **2017**, *17*, 7102−7109.
(49) Wang, Z.; Jia, H.; Yao, K.; Cai, W.; Chen, H.; Liu, Y. Circular Dichroism Metamirrors with Near-Perfect Extinction. *ACS Photonics* **2016**, *3*, 2096−2101.
(50) García-Guirado, J.; Svedendahl, M.; Puigdollers, J.; Quidant, R. Enantiomer-Selective Molecular Sensing Using Racemic Nanoplasmonic Arrays. *Nano Lett.* **2018**, *18*, 6279−6285.
(51) Yao, K.; Zheng, Y. Near-Ultraviolet Dielectric Metasurfaces: from Surface-Enhanced Circular Dichroism Spectroscopy to Polarization-Preserving Mirros. *J. Phys. Chem. C* **2019**, *123*, 11814−11822.

https://doi.org/10.1021/acsphotonics.2c01397
ACS Photonics 2023, 10, 155−161